Book Chapter

A Sufficient Condition for Small-Signal Synchronization Stability with Applications to PLL-Dominated Oscillation Mode Analysis

Guanzhong Wang*

Key Laboratory of Power System Intelligent Dispatch and Control of Ministry of Education, School of Electrical Engineering, Shandong University, Jinan 250061, China

***Corresponding Author:** Guanzhong Wang, Key Laboratory of Power System Intelligent Dispatch and Control of Ministry of Education, School of Electrical Engineering,Shandong University, Jinan 250061, China

Published **December 09, 2024**

This Book Chapter is a republication of an article published by Guanzhong Wang, et al. at International Journal of Electrical Power & Energy Systems in February 2024. (Qianhong Shi, Guanzhong Wang, Lei Ding, Zhijun Wang, Wei Wang, A sufficient condition for small-signal synchronization stability with applications to PLL-dominated oscillation mode analysis, International Journal of Electrical Power & Energy Systems, Volume 157, 2024, 109882, ISSN 0142-0615, https://doi.org/10.1016/j.ijepes.2024.109882. (https://www.sciencedirect.com/science/article/pii/S0142061524001030))

How to cite this book chapter: Guanzhong Wang. A Sufficient Condition for Small-Signal Synchronization Stability with Applications to PLL-Dominated Oscillation Mode Analysis. In: Wenping Zhang, editor. Top 10 Contributions in Energy Research. Hyderabad, India: Academic Reads. 2024.

Acknowledgments: This work was supported by the National Natural Science Foundation of China under Grant U23B20128, Grant U22B20101 and Grant 52007163.

Abstract

Small-signal instability in a wide frequency range due to the dynamic interaction between converters and the AC grid has attracted wide attention in recent years. Various impedance/admittance-based analysis methods are frequently adopted to resolve such problems. However, the stability criterion of the heterogeneous multi-converter system is not visually straightforward with admittance-based methods, because the complex coupling between admittances makes the stability criterion very difficult to be reduced. To overcome the shortcomings of those methods, an eigenvalue-free small-signal stability criterion is proposed by introducing the numerical range and Gershgorin discs theorem into the admittance model of multi-converter systems. By using Gershgorin discs to cover the numerical range of the system frequency domain admittance matrix, a transfer function of a single-input and single-output (SISO) system with variable weights is induced to perform the eigenvalue-free small-signal stability criterion, which provides a simple sufficient condition for system stability. Moreover, the SISO system is a weighted sum of admittances of heterogeneous converters, which illustrates that the stability of a heterogeneous multi-converter system is a tradeoff for heterogeneous single-converter systems. Finally, the effectiveness of the proposed method is demonstrated through eigenvalue analysis and simulation results based on a multi-converter test system.

Keywords

Small-Signal Stability; Multi-Converter System; Gershgorin Discs; Admittance Convex Combination

1. Introduction

With the large-scale integration of renewables, flexible AC transmission systems (FACTS) and high-voltage DC (HVDC) systems, growing penetration of voltage source converters (VSCs) emerges in modern power systems, and converter-dominated power systems will be the future [1]. However, small-signal instability in a wide frequency range has been observed frequently in converter-dominated power systems, which can lead to converter tripping, load shedding or system collapse [2]. Therefore, the study of analyzing and mitigating oscillations has raised considerable attention from academia and industry [3].

In traditional power systems, synchronous generators (SGs) synchronize with the AC grid via physical rotating motion, while in the converter-dominated power systems, currently almost all the VSCs operated in grid-following mode utilize a phase-locked loop (PLL) for grid synchronization [4]. As the PLL-synchronization mechanism is different from the physical synchronization mechanism of SGs, control interactions of VSCs will be stronger than those of SGs under high grid admittance (i.e., weak grid condition) [5]. Strong control interaction between the PLL and other control loops has been identified as the most potential cause for oscillation events over the past few years [6-9]. However, because of the large number of converters and the diversity of control configurations in heterogeneous multi-converter system, oscillation risk assessment of converter-dominated power systems in practice still encounters great challenges [10].

A linear approximate model with selective equilibriums of large-scale nonlinear power systems is widely used in oscillation analysis. That is because the oscillation of small-signal instability is always observed around a certain equilibrium of a power system. For multi-converter systems, the oscillation analysis methods based on the linear approximate model can be divided into two categories: the state-space method and the admittance method [11]. The state-space modelling combined with participation factor-based approach is first used to analyse the effect of PLL and short circuit ratio (SCR) on the small-

signal stability of a VSC-HVDC converter connected to a weak grid [5]. Also, interactions between the PLL of the rotor side converter of the double-fed induction generator (DFIG) and the AC grid are analysed and controlled via the state-space method [12]. For a wind farm of permanent magnet synchronous generators (PMSGs) under a weak grid connection, based on the character analysis of the reduced-order state-space model, the potential instability risk due to the PLL-dominated oscillation can be evaluated analytically with the collective parameters of PLLs of the PMSGs [13]. Thus far, the effectiveness of the state-space method in analysing and mitigating the oscillation relevant to PLL has relied on the detailed white-box model of converters so that the modal analysis can be performed.

However, the state-space model involves the disclosure of the internal design and the control apparatuses of converters, which cannot preserve commercially confidential detail, especially for the fact that the model of a converter is not as standardized as the model of a synchronous generator. To address the above shortcomings, admittance methods, as black-box models of converters, have played a significant role in oscillation analysis [14-17]. Admittances are in essence transfer function models of converters where the port is usually selected on the electrical side with voltage inputs and current outputs. The input-output relation is selected depending on the observability of the modes over the ports, i.e., the PLL-relevant modes are more observable on the electrical side. Besides, the coordinate frame in which the voltages and currents are observed can sort different admittance methods, e.g., sequence domain admittance model, dq domain admittance model, and phasor domain admittance model [18]. For single-converter systems, design-oriented single-input and single-output (SISO) admittance or transfer functions can be induced from different admittance models [19], with which the single-converter system's stability margin can be easily identified by the Nyquist stability criterion.

Then, for multi-converter systems, loci of determinant or eigenvalues of the return-ratio matrix (RRM) or return-difference matrix (RDM) are used to identify the system's stability margin [20], which are not visually straightforward

because the complex coupling between admittances makes the stability criterion very difficult to be reduced to an analytical SISO transfer function. For instance, the settling angle-based stability criterion for multi-converter systems is proposed by [21], where the determinant of RRM or RDM of the admittance of the whole system is used to perform the reduced Nyquist criterion. On the other hand, grid strength indices based on the eigenvalue decomposition of RDM, i.e., generalized SCR (gSCR) [22], can be used to approximate the stability margin of multi-converter systems by calculating the distance between the gSCR and its critical value. However, the validation of the grid strength-based stability criterion is limited to inhomogeneous converters that have similar control loops and parameters [23]. Consequently, the stability criteria for heterogeneous multi-converter systems still lack physical meaning, and reduced stability criteria are more limited in practical applications.

In this paper, an eigenvalue-free small-signal stability criterion for PLL-synchronization instability in heterogeneous multi-converter systems is presented. The major contributions of the paper can be summarized as follows:

1) The influence mechanism of each device on the system stability is clarified through the analytical formula of device weighting, and the stability criterion of the heterogeneous multi-converter system is proved equal to that of a system composed of the weighted sum of these different converters in the heterogeneous multi-converter system. Thus, the eigenvalue-free small-signal stability criterion illustrates that the stability of a heterogeneous multi-converter system can be seen as a trade-off of heterogeneous single-converter systems.

2) Inspired by the negative incremental resistor produced by the PLL [14], a reduced admittance model of the heterogeneous multi-converter system is constructed. By introducing the Gershgorin discs theorem [24] to cover the numerical range of the system node admittance matrix, the proposed criterion significantly reduces the complexity of small-signal stability analysis of heterogeneous multi-converter systems and improves the practical applicability.

3) Furthermore, introducing the transfer function of the SISO system with variable weights to perform the Nyquist stability criterion provides a simple sufficient condition for small-signal stability, but is less conservative. The effectiveness of the proposed method is verified by modal analysis and time domain simulation of a multi-converter test system.

The rest of this paper is organized as follows. In Section 2, the admittance model and order reduction procedure of heterogeneous multi-converter systems are described. Then, a stability analysis method based on the numerical range and Gershgorin discs is performed in Section 3, where an eigenvalue-free small-signal stability criterion is proposed. Subsequently, the simulation results are presented in Section 4 to confirm the effectiveness of the theoretical analysis. Finally, the conclusions are drawn in Section 5.

2. Small-Signal Stability Analysis Model

Different from the SG which has a rotating mass, converters usually synchronize with the AC grid through the PLL, which provides a synchronous phase by tracking the terminal voltage. Therefore, this paper takes the frequency domain admittance model of a VSC-based heterogeneous multi-converter system as an example. The grid-connected VSC system is shown in Fig. 1, tin which the reactive power outer loop adopts constant reactive power control, and the active power outer loop considers two control methods: constant DC voltage and constant active power.

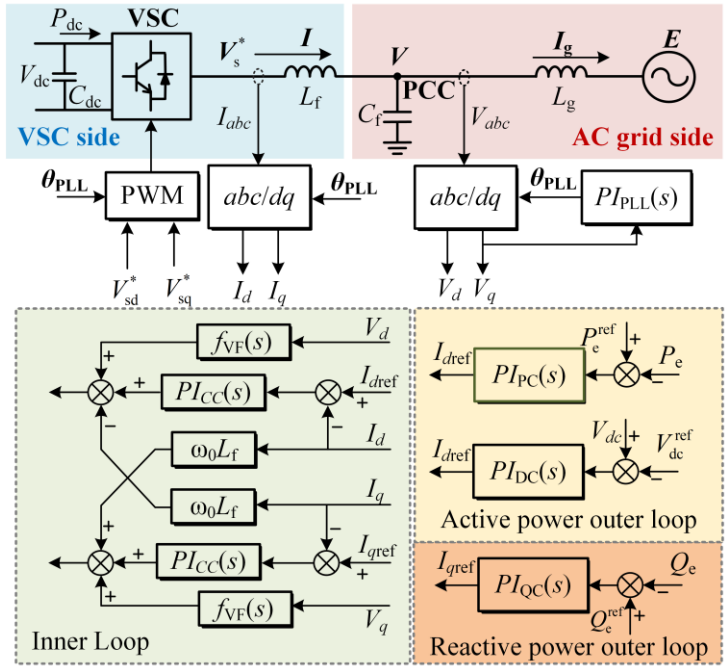

Figure 1: Grid-connected VSC and its control diagram.

2.1. Converter Dynamics and Control Strategy

The admittance matrix of the LCL filter on the AC grid side of the converter and the current inner loop under the dq axis is symmetrical. For the convenience of expression, this paper uses a complex transfer function to describe this part of the dynamics.

$$\dot{V} - \dot{E} = \left(sL_g + j\omega L_g\right)\dot{I}_g \tag{1}$$

$$\dot{I} - \dot{I}_g = \left(sC_f + j\omega C_f\right)\dot{V} \tag{2}$$

$$\dot{V}_s^* - \dot{V} = \left(sL_f + j\omega L_f\right)\dot{I} \tag{3}$$

$$\dot{V}_s^* = PI_{CC}\left(\dot{I}^{ref} - \dot{I}\right) + j\omega L_f \dot{I} + f_{VF}(s)\dot{V} \tag{4}$$

where, s is the Laplace operator; L_f is the VSC side filter inductance, L_g is the AC grid side inductance, C_f is the filter capacitor, $PI_{CC}(s)=K_{CCP}+K_{CCI}/s$ is the current inner loop PI controller transfer function, $\dot{I}^{ref}=I_q^{ref}+jI_q^{ref}$ is the complex number of the inner loop current reference value, the rest of the variables with the same arrow sign are all complex numbers in the same form as $\dot{I}^{ref}$, and $f_{VF}(s)=K_{VF}/(T_{VF}s+1)$ is a voltage feedforward low-pass filter.

The admittance matrixes of the PLL and the outer loop are not symmetrical, so their transfer functions in the scalar form need to be listed separately. The dynamic equation of the PLL is as follows:

$$\theta=\frac{\omega}{s}=\frac{1}{s}\left(PI_{PLL}(s)V_q+\omega_0\right) \tag{5}$$

where, $PI_{PLL}(s)=K_{PLL}+K_{PLL}/s$ is the PI controller transfer function of the PLL, θ and ω is the output phase and frequency of the PLL, and ω_0 represents the system power frequency.

Both the constant reactive power outer loop and the constant active power outer loop complete the closed-loop control by measuring the AC grid side power signal. Since their forms are similar, their dynamic equations can be combined and written as follows:

$$I_d^{ref}=PI_{PC}(s)\left(f_{PQ}(P_e)-P_e^{ref}\right) \tag{6}$$

$$I_q^{ref}=PI_{QC}(s)\left(f_{PQ}(Q_e)-Q_e^{ref}\right) \tag{7}$$

where, $PI_{PC}(s)=K_{PCP}+K_{PCI}/s$ is the transfer function of active outer loop PI controller, $PI_{QC}(s)=K_{QCP}+K_{QCI}/s$ is the transfer function of reactive outer loop PI controller, $f_{PQ}(s)=K_{PQ}/(T_{PQ}s+1)$ is the low-pass filter of the power measurement link.

The constant DC voltage outer loop dynamically couples the active power control of the AC grid side with the capacitor

voltage of the DC side. Therefore, in the stability analysis, since the DC side capacitance is much larger than the filter capacitor, it is necessary to consider the dynamics of the DC side capacitance. The dynamic equation is as follows:

$$I_{\mathrm{d}}^{\mathrm{ref}} = PI_{\mathrm{DC}}(s)\left(V_{\mathrm{dc}} - V_{\mathrm{dc}}^{\mathrm{ref}}\right) \tag{8}$$

$$V_{\mathrm{dc}} C_{\mathrm{dc}} s V_{\mathrm{dc}} = P_{\mathrm{r}} - P_{\mathrm{e}} \tag{9}$$

In addition, the power calculation equations can be calculated:

$$P_{\mathrm{e}} = V_{\mathrm{d}} I_{\mathrm{d}} + V_{\mathrm{q}} I_{\mathrm{q}} \tag{10}$$

$$Q_{\mathrm{e}} = -V_{\mathrm{d}} I_{\mathrm{q}} + V_{\mathrm{q}} I_{\mathrm{d}} \tag{11}$$

where, P_{r} is the input power of the DC bus, and the dynamics of the input power is ignored here, and it is regarded as a constant; Q_{e} and P_{e} are the reactive power and active power of the three-phase circuit on the AC grid side, respectively.

2.2. Frequency Domain Admittance Matrix Characteristics Analysis

In practice, the reactive power compensation provided by renewable energy sources is little, so the power factor of the VSC can be considered as 1; meanwhile, the PLL-dominated synchronous stability problem mainly occurs in the 10~100Hz frequency band, while the participation of the AC grid side filter capacitor is extremely little in the low and medium frequency bands, thus the capacitive circuit in this part can be neglected.

By linearizing equations (1)-(11), the frequency domain admittance matrix that reflects the relationship between the voltage amplitude/phase and current amplitude/phase at the AC grid side of the converter can be obtained by (Suppose the current flowing into the converter is in the positive direction, see Appendix A for specific derivation):

$$\begin{bmatrix} \Delta I \\ I\Delta\varphi \end{bmatrix} = \underbrace{\begin{bmatrix} Y_{g1}(s) & \\ & Y_{g4}(s) \end{bmatrix}}_{\boldsymbol{Y}_{VSC}(s)} \begin{bmatrix} \Delta V \\ V\Delta\theta \end{bmatrix} \tag{12}$$

where, θ and φ represent the phase angles of the port voltage and current in the global reference *xy* frame respectively; $\boldsymbol{Y}_{VSC}(s)$ is the frequency domain admittance matrix in polar coordinates, $Y_{g1}(s)$ indicates the magnitude loop: $\Delta V \to \Delta I$, and $Y_{g4}(s)$ indicates the phase loop: $V\Delta\theta \to I\Delta\varphi$, its specific elements are as follows:

$$\begin{cases} Y_{g1}(s) = \dfrac{G_{VF}(s) + G_I(s)G_{APC}(s)I_{d0}}{G_I(s)G_{APC}(s)V_{d0} + 1} \\ Y_{g4}(s) = \dfrac{G_{VF}(s)(1 - V_{d0}G_{PLL}(s))}{G_I(s)G_{RPC}(s)V_{d0} + 1} - \dfrac{(G_{RPC}(s) + G_{PLL}(s))G_I(s)I_{d0}}{G_I(s)G_{RPC}(s)V_{d0} + 1} \end{cases} \tag{13}$$

where, the subscript '0' of the physical quantity indicates the steady-state value of the physical quantity: $V_{d0} = 1.0\text{p.u.}$, $I_{d0} = 1.0\text{p.u.}$, etc.; the transfer function G_{xx} in (13) is given as below:

$$\begin{cases} G_{PLL}(s) = \dfrac{PI_{PLL}(s)}{s} / (1 + \dfrac{PI_{PLL}(s)V_{d0}}{s}) \\ G_{RPC}(s) = PI_{QC}(s)\, f_{PQ}(s) \\ G_{VF}(s) = (1 - f_{VF}(s))/(sL_f + PI_{CC}(s)) \\ G_I(s) = PI_{CC}(s) / (sL_f + PI_{CC}(s)) \\ G_{APC}(s) = \begin{cases} PI_{DC}(s) / sV_{dc0}C_{dc}, \text{ Constant DC voltage outer loop} \\ PI_{PC}(s)\, f_{PQ}(s), \text{ Constant active power outer loop} \end{cases} \end{cases} \tag{14}$$

In order to analyze the synchronous stability mechanism with small disturbance, find vital factors and analyze the interaction between matrix elements, it is necessary to simplify the frequency domain admittance matrix:

- Only retain $Y_{g4}(s)$ representing the phase loop;
- Neglect the phase angle difference of different converter grid-connected buses.

Here is an illustration of the rationality of the above simplifications:

According to (13), it is seen that the PLL transfer function only appears in the element $Y_{g4}(s)$. In addition, according to the actual operation data of the East China Power Grid, the phase angle deviation between buses is generally less than 10°, thus, by considering that the capacity of the converter is much smaller than that of SG, the phase angle difference of 5° is taken as a reference value and substituted into the following frequency-domain admittance matrix model of the open-loop system of the converter [22]:

$$\begin{cases} \begin{bmatrix} \Delta I \\ I\Delta\varphi \end{bmatrix} = \boldsymbol{Y}_g \begin{bmatrix} \Delta V \\ V\Delta\theta \end{bmatrix} \\ \boldsymbol{Y}_g = \boldsymbol{T}^{-1} \begin{bmatrix} Y_{g1}(s) & \\ & Y_{g4}(s) \end{bmatrix} \boldsymbol{T} = \begin{bmatrix} Y_{g(1,1)}(s) & Y_{g(1,2)}(s) \\ Y_{g(2,1)}(s) & Y_{g(2,2)}(s) \end{bmatrix} \\ \boldsymbol{T} = \begin{bmatrix} \cos\theta & \sin\theta \\ -\sin\theta & \cos\theta \end{bmatrix} \end{cases} \tag{15}$$

where $\boldsymbol{T}$ is the frame rotation matrix, which specifically represents the transformation from the *dq* rotation reference frame of the controller to the global *xy* rotation reference frame, and θ is the voltage phase angle of the converter bus. The parameters required are shown in Table 1.

Table 1: Parameters of converter controller.

Symbols	Descriptions	Values
L_f	Filter inductor	0.05p.u.
$PI_{DC}(s)$	DC voltage outer loop transfer function	10+4/s
$PI_{PC}(s)$	Active power outer loop transfer function	0.3+5/s
$PI_{QC}(s)$	Reactive power outer loop transfer function	0.3+5/s
$PI_{cc}(s)$	Current inner loop transfer function	1+10/s
$PI_{PLL}(s)$	PLL transfer function of VSC	8+7800/s
$f_{VF}(s)$	Voltage feed-forward low-pass filter	1/(1+0.01s)
$f_{PQ}(s)$	Power measurement low-pass filter	1/(1+0.001s)
P, *Q*	Active and reactive power output	1p.u.,0p.u.

The bode diagrams of $\boldsymbol{Y}_{\mathrm{g}}$ under different outer loop control modes are drawn below. As shown in the blue area in Fig. 2, in the sub/supersynchronous oscillation frequency band (10Hz~100Hz) dominated by PLL, the amplitude of the phase loop $Y_{\mathrm{g}(2,2)}(s)$ is greater than 0 dB, and the amplitudes of the other elements in $\boldsymbol{Y}_{\mathrm{g}}$ are less than 0 dB. Therefore, $Y_{\mathrm{g}(2,2)}(s)$ becomes the dominant oscillation link and provides a larger negative resistance.

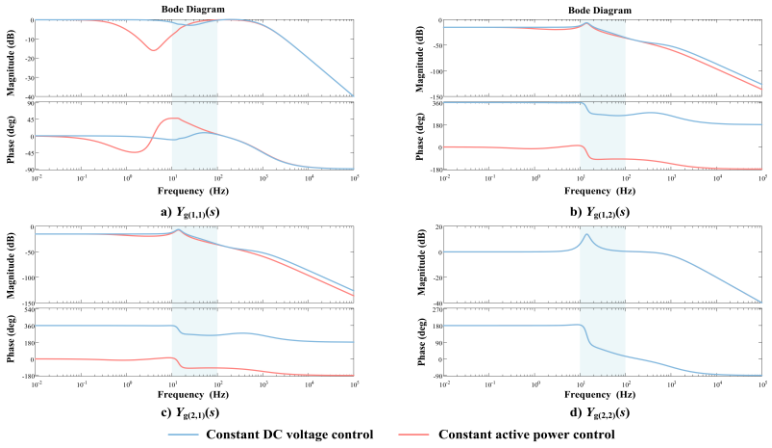

Figure 2: Bode plot of converter open-loop system.

The above analysis proves the validity of the assumptions used in this paper.

Using the frequency domain admittance matrix of the multi-converter system in [22], and recombining its matrix elements, the approximated frequency domain admittance matrix $\boldsymbol{Y}_{\mathrm{sys}}$ of the multi-converter system can be obtained as follows:

$$\begin{bmatrix} \boldsymbol{Y}_{\mathrm{g1}}+\boldsymbol{B}\alpha(s) & \boldsymbol{B}\beta(s) \\ -\boldsymbol{B}\beta(s) & \boldsymbol{Y}_{\mathrm{g4}}+\boldsymbol{B}\alpha(s) \end{bmatrix} \approx \begin{bmatrix} \boldsymbol{B}\alpha(s) & \boldsymbol{B}\beta(s) \\ -\boldsymbol{B}\beta(s) & \boldsymbol{Y}_{\mathrm{g4}}+\boldsymbol{B}\alpha(s) \end{bmatrix} = \boldsymbol{Y}_{\mathrm{sys}} \tag{16}$$

where, the specific expressions of the scalar functions $\alpha(s)$ and $\beta(s)$ are $s\omega_0/\left(s^2+\omega_0^2\right)$ and $\omega_0^2/\left(s^2+\omega_0^2\right)$ separately; $\boldsymbol{B}$ and $\boldsymbol{Y}_{\mathrm{g4}}$ are both matrices, the former is the node admittance matrix of the

multi-converter system, and the latter is a diagonal matrix formed by the admittance elements of the individual converters, more details are shown in (17) and (18).

$$\boldsymbol{B}=\begin{bmatrix} B_{11} & B_{12} & \mathrm{K} & B_{1n} \\ B_{21} & B_{22} & \mathrm{K} & B_{2n} \\ \mathrm{M} & \mathrm{M} & \mathrm{M} & \mathrm{M} \\ B_{n1} & B_{n2} & \mathrm{K} & B_{nn} \end{bmatrix} \tag{17}$$

$$\boldsymbol{Y}_{\mathrm{g4}}(s)=diag(Y_{\mathrm{g4,1}}(s),\mathrm{K},Y_{\mathrm{g4,n}}(s)) \tag{18}$$

where, $diag(\mathrm{g})$ represents a diagonal matrix, and the diagonal elements are in parentheses; the elements of $\boldsymbol{B}$ are real numbers in terms of per-unit values, and the diagonal elements are positive.

The stability of the multi-converter system can be analyzed by using the determinant of the frequency domain admittance matrix $\boldsymbol{Y}_{\mathrm{sys}}$, that is, to solve the polynomial about s represented by (19). If the real part of s obtained is all negative, then the multi-converter system is stable with small disturbance, and vice-versa, the system is unstable.

$$\det\left(\boldsymbol{Y}_{\mathrm{sys}}\right)=0 \tag{19}$$

By further observing the structure of the system frequency domain admittance matrix $\boldsymbol{Y}_{\mathrm{sys}}$ in (15), and according to $\det\left(\boldsymbol{B}\alpha(s)\right)\neq 0$, the equivalent condition of (19) can be obtained:

$$\det\left(\boldsymbol{Y}_{\mathrm{sys}}\right)=0 \Leftrightarrow \det\left(\boldsymbol{Y}_{\mathrm{g4}}(s)+\boldsymbol{B}\left(\alpha(s)+\alpha(s)^{-1}\beta(s)^{2}\right)\right)=0 \tag{20}$$

The reduced-order admittance matrix of multi-converter system $\boldsymbol{Y}_{\mathrm{sys0}}$ is recorded as:

$$\boldsymbol{Y}_{\mathrm{sys0}}(s)=\boldsymbol{Y}_{\mathrm{g4}}(s)+\boldsymbol{B}\left(\alpha(s)+\alpha(s)^{-1}\beta(s)^{2}\right) \tag{21}$$

In the following, the analytical expression of the eigenvalue trajectory cluster of the multi-converter system will be deduced according to the equivalence condition (20), combined with the application of the numerical range and the Gershgorin Discs theorem.

3. Eigenvalue-Free Small-Signal Stability Criterion Of PLL-Based VSC

The stability of the multiple input multiple output (MIMO) system is mainly analyzed through the Generalized Nyquist Criterion (GNC), which is essential whether the Nyquist curve of the eigenvalues of the frequency domain admittance matrix $\boldsymbol{Y}_{sys0}(s)$ encloses the (0, j0) point. In practice, the complex numbers corresponding to different frequencies are substituted into s to obtain all the eigenvalues of $\boldsymbol{Y}_{sys0}(s)$, and then connected frequency by frequency to form multiple interwoven Nyquist curves. Although the physical meaning of the admittance method itself is clear, the GNC relies on a point-by-point eigenvalue decomposition of a high-dimensional matrix over a wide frequency band and therefore is not available in analytic form, which results in a stability criterion that is only indicative of the stability of the system and lacks the necessary physical interpretation.

Because of the above problems, this section first simplifies the eigenvalue trajectory cluster of the reduced-order admittance matrix $\boldsymbol{Y}_{sys0}$ through the numerical range, and then uses the Gershgorin Discs to cover the numerical range of the node admittance matrix on the AC grid side to achieve a SISO transfer function or the eigenvalue-free stability criterion. Finally, the physical meaning of the eigenvalue-free small-signal stability criterion of the multi-converter system is explained by using the subordination relationship between the Gershgorin discs and the numerical range.

3.1. Numerical Range Criterion

The numerical range is a widely used tool for matrix analysis, as described in Definition 1.

Definition 1 [24]: Define the complex number set $x^*\boldsymbol{A}x$ as the numerical range $F(A)$ of matrix $\boldsymbol{A}$, and the norm of the vector x is equal to 1, that is, $\|x\|=1$. $F(A)$ can be calculated by:

$$F(\boldsymbol{A})=\left\{x^*\boldsymbol{A}x \mid x\in £^n, \|x\|=1\right\} \tag{22}$$

where $£^n$ is an n-dimensional complex vector field, and the superscript * represents the conjugate operation.

The general properties of the numerical range defined by (22) are introduced through Lemma 1.

Lemma 1: Assuming that $\boldsymbol{A}$ is a $n\times n$ complex square matrix, the following three conditions are satisfied:

- If $\boldsymbol{A}_k$ is any main submatrix of $\boldsymbol{A}$, then $F(A_k)\subseteq F(A)$ is established;
- $F(A)$ contains all of the eigenvalues of $\boldsymbol{A}$;
- $F(A)$ contains all of the diagonal entries of $\boldsymbol{A}$.

The proof process of Lemma 1 can be found in [24]. The purpose of introducing Lemma 1 in this paper is to explain that the GNC of the system frequency domain admittance matrix is all subordinate to the numerical range of the matrix. It is worth noting that when the $\boldsymbol{A}$ is a normal matrix, the numerical range $F(A)$ of $\boldsymbol{A}$ is the convex hull of its eigenvalues [25], hence, the following relationship exists:

$$\lambda\in\sigma(A)=F(A) \tag{23}$$

where, λ is the eigenvalue of $\boldsymbol{A}$, and $\sigma(A)$ is the whole of all eigenvalues of $\boldsymbol{A}$, which is called spectrum.

In this part, the numerical range criterion for the PLL oscillation mode of the multi-converter system will be illustrated in the form of conclusions. First, let $\lambda(\boldsymbol{B})$ be the eigenvalue set of $\boldsymbol{B}$.

Conclusion 1: For the small-signal stability analysis model represented by the reduced-order admittance matrix $\boldsymbol{Y}_{sys0}$ of the

multi-converter system, the Nyquist curve of each device $Y_{g4,i}(s)\lambda_{min}^{-1}(\boldsymbol{B})/(\alpha(s)+\alpha(s)^{-1}\beta(s)^2)$ in the system does not surround the (-1, j0) point can be a sufficient condition for the small-signal stability of the system.

Then, the derivation process of Conclusion 1 is shown below. According to the conditions in Lemma 1, the eigenvalue $\lambda(\boldsymbol{Y}_{sys0})$ of $\boldsymbol{Y}_{sys0}$ satisfy the following conditions:

$$\lambda(\boldsymbol{Y}_{sys0}) \subset \left\{ \sum \gamma_i Y_{i4,i}(s) + \varsigma\left(\alpha(s)+\alpha(s)^{-1}\beta(s)^2\right) \mid \sum \gamma_i = 1, \varsigma \in \left[\lambda_{min}(\boldsymbol{B}), \lambda_{max}(\boldsymbol{B})\right] \right\} \quad (24)$$

where, γ_i is the weighting coefficient of the device admittance element $Y_{g4,i}$, which satisfies $\sum \gamma_i = 1$ and $\gamma_i \geq 0$; $\sum \gamma_i Y_{g4,i}(s)$ is the numerical range of the converter admittance, which is also a convex combination of $\boldsymbol{Y}_{g4}(s)$ diagonal elements; $\varsigma\left(\alpha(s)+\alpha(s)^{-1}\beta(s)^2\right)$ is the numerical range of the AC side matrix $\boldsymbol{B}\left(\alpha(s)+\alpha(s)^{-1}\beta(s)^2\right)$, by using Lemma 1 and the numerical range properties of normal matrix $\boldsymbol{B}$, it can be obtained that $\varsigma \in \left[\lambda_{min}(B), \lambda_{max}(B)\right]$, where $\lambda_{min}(\boldsymbol{B})$ and $\lambda_{max}(\boldsymbol{B})$ represent the minimum and maximum eigenvalues of $\boldsymbol{B}$, respectively.

It is worth mentioning that the smaller ς is, the worse the small-signal stability of the system is [23]. To simplify the analysis process, $\varsigma = \lambda_{min}(\boldsymbol{B})$ can be set to obtain a sufficient condition for the system's small-signal stability. In addition, it is necessary to note that $Y_{g4,i}(s) + \lambda_{min}(\boldsymbol{B})(\alpha(s)+\alpha(s)^{-1}\beta(s)^2)$ is also the pole of the convex combination $\sum \gamma_i Y_{g4,i}(s) + \lambda_{min}(\boldsymbol{B})(\alpha(s)+\alpha(s)^{-1}\beta(s)^2)$, so the Nyquist curve of each converter $Y_{g4,i}(s)\lambda_{min}^{-1}(\boldsymbol{B})/(\alpha(s)+\alpha(s)^{-1}\beta(s)^2)$ in the system does not surround the (-1, j0) point, which can be used as a sufficient condition for assessing the small-signal stability of the multi-converter system.

However, as the scale of the power grid becomes larger, the order of the node admittance matrix $\boldsymbol{B}$ will become higher, and it

will be more difficult to calculate the eigenvalues, which loses the advantages of simplicity and convenience of the numerical range method.

3.2. Eigenvalue-Free Small-Signal Stability Criterion

Gershgorin disk theorem is widely used in the estimation and location of eigenvalues of matrices. In order to reduce the computational burden caused by solving the eigenvalues of the high-dimensional matrix, this section uses the Gershgorin disk theorem to cover the numerical range of the system node admittance matrix ***B***. For a $n \times n$ square matrix, there are *n* row disks and column disks, and their eigenvalues are located in these discs. The specific definition is shown below:

Definition 2 [24]**:** Assuming that ***A*** is a $n \times n$ complex square matrix, the closed discs can be expressed as:

$$G^{(i)}(A) = \left\{ | z - a_{ii} | \leq R_i^{'}(A) \right\} \subset £, \forall i = 2,...,n \tag{25}$$

where, $R_i^{'}(A) = \sum_{j \neq i} \left| a_{ij} \right|$ is interpreted as the row sum, are called the Gershgorin discs, £ is the complex plane, and $G(\mathrm{A}) = \mathrm{U}_{i=1}^{n} G^{(i)}(\mathrm{A})$ is the Gershgorin region.

The following lemma introduces the general properties of the Gershgorin region defined by (25).

Lemma 2: Assuming that ***A*** is a $n \times n$ complex square matrix, then the relation $\sigma(A) \subset G(A) \cap G(A^T)$ holds.

The proof process of Lemma 2 can be found in [24]. This lemma states that any eigenvalue of ***A*** is in both row and column disks. When ***A*** is a symmetric normal matrix, its eigenvalues are all real numbers, and the inclusion relationship of the three ranges, i.e., the numerical range, Gershgorin region and eigenvalue range of ***A*** is $\lambda \in \sigma(A) = F(A) \subset G(A) \cap G(A^T)$, as shown in Fig. 3.

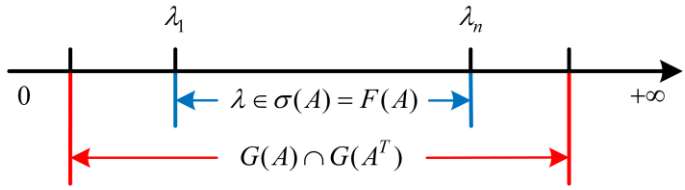

Figure 3: Relationship among the three ranges

The purpose of introducing the Gershgorin discs in this paper is to illustrate that the numerical range of the system node admittance matrix $\boldsymbol{B}$ is all subject to the Gershgorin region of $\boldsymbol{B}$. Based on this, the eigenvalue-free small-signal stability criterion of the PLL-based VSC in multi-converter systems can be constructed. First, let $G(\boldsymbol{B})$ be the distance from the boundary of Gershgorin region of $\boldsymbol{B}$ to the origin. Then, the eigenvalue-free small-signal stability criterion described by the following conclusion can be obtained.

Conclusion 2: For the small-signal stability analysis model of the multi-converter system represented by $\boldsymbol{Y}_{\text{sys0}}$ in (20), the Nyquist curve of each device $Y_{\text{g4,i}}(s)/G_{\min}(\boldsymbol{B})(\alpha(s)+\alpha(s)^{-1}\beta(s)^2)$ in the system does not surround the (-1, j0) point can be a sufficient condition for the stability of the system.

Then, the derivation process of Conclusion 2 is shown below. According to the Lemma 1 and Lemma 2, all eigenvalues of the normal matrix $\boldsymbol{B}$ will lie in the Gershgorin region of $\boldsymbol{B}$, hence, the eigenvalue $\lambda(\boldsymbol{Y}_{\text{sys0}})$ of $\boldsymbol{Y}_{\text{sys0}}$ satisfy the following conditions:

$$\lambda(\boldsymbol{Y}_{\text{sys0}}) \subset \left\{ \sum \gamma_i Y_{\text{i4,i}}(s) + k\left(\alpha(s)+\alpha(s)^{-1}\beta(s)^2\right) \middle| \sum \gamma_i = 1, k \in \left[G_{\min}(\boldsymbol{B}), G_{\max}(\boldsymbol{B})\right] \right\} \quad (26)$$

where, γ_i is the weighting coefficient of the device admittance element $Y_{\text{g4,i}}$, which satisfies $\sum \gamma_i = 1$ and $\gamma_i \geq 0$; $k\left(\alpha(s)+\alpha(s)^{-1}\beta(s)^2\right)$ is the numerical range of $\boldsymbol{B}\left(\alpha(s)+\alpha(s)^{-1}\beta(s)^2\right)$. According to the Gershgorin discs, it can be obtained that $k \in \left[G_{\min}(B), G_{\max}(B)\right]$, where $G_{\min}(\boldsymbol{B})$ and

$G_{\max}(\boldsymbol{B})$ represent the closest distances of the minimum and maximum Gershgorin region boundaries of $\boldsymbol{B}$ to the origin, respectively.

Similar to the proof process of Conclusion 1, setting $k = G_{\min}(\boldsymbol{B})$ obtains a sufficient condition for the stability of the system with small disturbance. Also, the $Y_{\mathrm{g4,i}}(s) + G_{\min}(\boldsymbol{B})(\alpha(s) + \alpha(s)^{-1}\beta(s)^2)$ is the pole of the convex combination $\sum \gamma_{\mathrm{i}} Y_{\mathrm{g4,i}}(s) + G_{\min}(\boldsymbol{B})(\alpha(s) + \alpha(s)^{-1}\beta(s)^2)$, so the Nyquist curve of each converter $Y_{\mathrm{g4,i}}(s) / G_{\min}(\boldsymbol{B})(\alpha(s) + \alpha(s)^{-1}\beta(s)^2)$ in the system does not surround the (-1, j0) point can be used as a sufficient condition to evaluate the small-signal stability of the multi-converter system.

It is critical to emphasize that the introduction of the Gershgorin discs theorem enables the proposed criterion to have the following properties:

- It is unnecessary to calculate the eigenvalues of the system frequency domain admittance matrix when analyzing the small-signal stability of the heterogeneous multi-converter systems;
- Decentralized computing can be achieved without global information due to that the Gershgorin discs of ***B*** can be calculated using local information of buses.

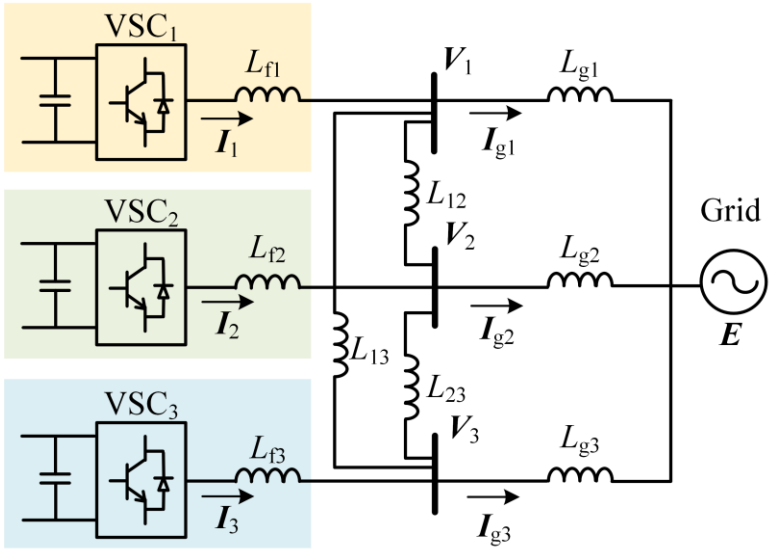

Figure 4: Multi-converter system.

To illustrate the decentralized computing process of the criterion, the node admittance matrix $\boldsymbol{B}$ of an equivalent simplified model of the multi-converter system shown in Fig. 4 is obtained as follows:

$$\boldsymbol{B}=\begin{bmatrix} \frac{1}{\omega L_{g1}}+\frac{1}{\omega L_{12}}+\frac{1}{\omega L_{13}} & -\frac{1}{\omega L_{12}} & -\frac{1}{\omega L_{13}} \\ -\frac{1}{\omega L_{12}} & \frac{1}{\omega L_{g2}}+\frac{1}{\omega L_{12}}+\frac{1}{\omega L_{23}} & -\frac{1}{\omega L_{23}} \\ -\frac{1}{\omega L_{13}} & -\frac{1}{\omega L_{23}} & \frac{1}{\omega L_{g3}}+\frac{1}{\omega L_{13}}+\frac{1}{\omega L_{23}} \end{bmatrix} \quad (27)$$

where, L_{gi} is the equivalent inductance between bus i and the AC grid, and L_{ij} is the connection inductance between bus i and bus j. Take the calculation of the Gershgorin discs of a certain row or column in $\boldsymbol{B}$ as an example, only inductances of lines connected to the bus corresponding to the diagonal element of matrix $\boldsymbol{B}$ are used, as shown in (28).

$$G^{(1)}(\boldsymbol{B})=\left\{|z-(\frac{1}{\omega L_{g1}}+\frac{1}{\omega L_{12}}+\frac{1}{\omega L_{13}})|\leq(\frac{1}{\omega L_{12}}+\frac{1}{\omega L_{13}})\right\} \tag{28}$$

To sum up, the criterion proposed in this paper only uses the local information of the multi-converter system, that is, $Y_{g4,i}(s)$ representing the dynamics of the converter phase loop and the row or column of the node admittance matrix $\boldsymbol{B}$. In practical engineering applications, it is easy to obtain $\boldsymbol{B}$. Therefore, the proposed criterion solves the problem of poor observability of GNC of high-dimensional matrices and provides the possibility of decentralized implementation.

3.3. The Significance of the Eigenvalue-Free Small-Signal Stability Criterion

First, it can be seen that in (26) that the admittance of the VSCs in the numerical range can be expressed as a convex combination of the admittance $Y_{g4,i}(s)$ of multiple PLL-based converters. This convex combination form of converters mathematically explains why the stability of the heterogeneous multi-converter system can be expressed as the result of a compromise between the stability of the single-converter systems of multiple heterogeneous converters [23]. In addition, the eigenvalue trajectory clusters of the multi-converter system are contained in the numerical range and reduced to a SISO transfer function with variable coefficients, therefore, when analyzing the small-signal stability of the heterogeneous multi-converter system, the proposed criterion can significantly reduce the computation of high-dimensional matrices. Finally, the eigenvalue-free small-signal stability criterion uses Gershgorin discs to converter the numerical range to perform a sufficient condition for the small-signal stability of the multi-converter system. Although it is conservative to a certain extent, it has obvious significance in the actual engineering application of the heterogeneous multi-converter systems.

4. Case Analysis

To verify the effectiveness of the proposed criterion, a small-signal analysis model of the double-converter system is carried out in Matlab/Simulink for case studies. Two-level voltage source converter (VSC) based on PLL synchronization is used as a source-side renewable energy type, which is mainly used in Type 4 Wind Turbine Generators, Photovoltaic Power Generators, and Voltage Source Converter based High Voltage Direct Current Transmission (VSC-HVDC). The topology and parameters of the simulation system are shown in Fig. 5 and Table 2, respectively.

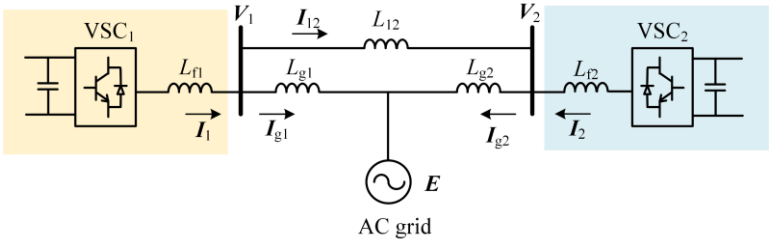

Figure 5: Schematic diagram of double-converter system.

Table 2: Parameters of double-converter system.

Symbols	Descriptions	Values
S, U_N	Rated capacity and voltage of the AC system	1500kVA, 690V
S_B	Rated capacity of power electronic device	1500kVA
V_{dc}	Rated voltage on the DC side	1100V
C_{dc}	Capacitance on the DC side	0.038p.u.
L_f	Inductance of the filter	0.05p.u.
R_{Line}	Resistance of the AC grid	0.05p.u.
L_g	Inductance of the AC grid	0.2pu
L_{12}	Mutual inductance of the AC grid	0.1pu
$PI_{PLL1}(s)$	PLL transfer function of VSC_1	26+7800/s
$PI_{PLL2}(s)$	PLL transfer function of VSC_2	36+3600/s

4.1. Validity Analysis of Eigenvalue-Free Small-Signal Stability Criterion

In this section, by comparing the influence of different stability criteria on system stability analysis under different power grid strengths, the effectiveness of the eigenvalue-free small-signal stability criterion is illustrated. According to Table 1, the system parameters of the two converters are set, and the grid-side node admittance matrix based on the p.u. value parameters is as follows:

$$\boldsymbol{B}=k_{\mathrm{B}}\begin{bmatrix} 15 & -10 \\ -10 & 15 \end{bmatrix} \tag{29}$$

where, k_{B} is parameter to adjust the grid strength of the system. Assuming k_{B}=1, at this time, the gSCR or the minimum eigenvalue of $\boldsymbol{B}$ of the system is set at approximately 5. According to engineering experience, under the condition of this gSCR, the system is stable with a small disturbance. The Nyquist curves of the eigenvalue-free small-signal stability criterion in the grid-connected system of the two converters are plotted according to Conclusion 2, as shown in Fig. 6. As can be seen, the Nyquist curves of eigenvalue-free small-signal stability criterion $Y_{\mathrm{g4},i}(s)/G_{\min}(\boldsymbol{B})(\alpha(s)+\alpha(s)^{-1}\beta(s)^{2})$ (i=1,2) corresponding to the heterogeneous converters VSC_1 and VSC_2 do not enclose the (-1,0) point, indicating that the system is stable. To verify the validity of the above results, the generalized Nyquist curves of the full-order frequency-domain admittance matrix of the double-converter system with $\boldsymbol{Y}_{\mathrm{g1}}$ in (16) are plotted in Fig. 7. It can be seen from Fig. 7 that the four generalized Nyquist curves also do not enclose the (-1,0) point, indicating that the system is stable. The above results demonstrate the effectiveness of the method proposed in this paper.

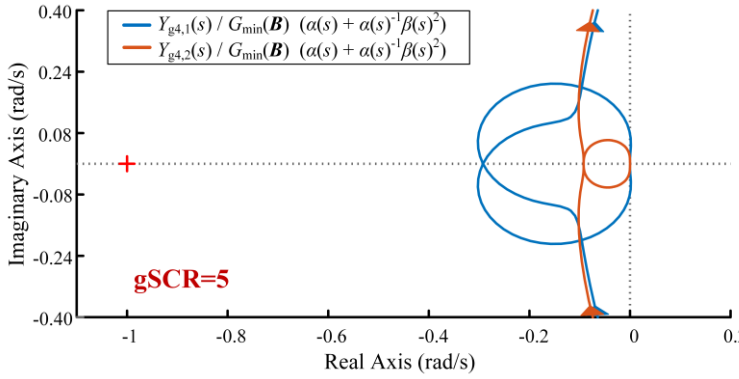

Figure 6: Eigenvalue-free small-signal stability criterion of double-converter system (gSCR=5).

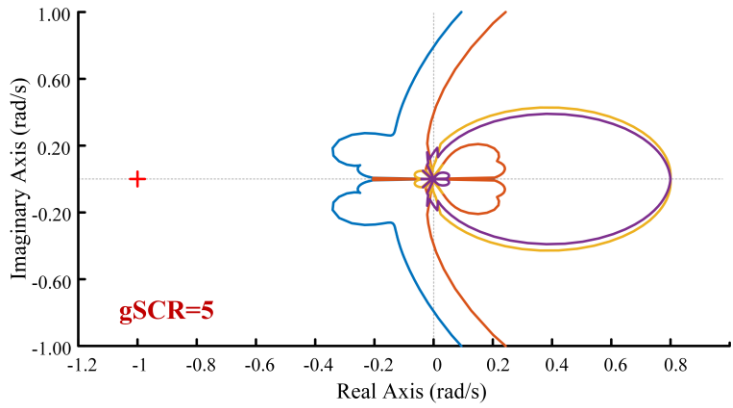

Figure 7: Generalized Nyquist curves of double-converter system (gSCR=5).

4.2. Conservativeness Analysis of Eigenvalue-Free Small-Signal Stability Criterion

Let $k_B = 0.28$, at this time, the gSCR of the system is set at 1.4, and the eigenvalue-free small-signal stability criterion and GNC are shown in Fig. 8 and Fig. 9, respectively. In this case, the eigenvalue-free small-signal stability criterion in Fig. 8 encloses the (-1, j0) point, and the system is unstable; However, all trajectories in Fig. 9 do not enclose the (-1, j0) point, the system is in a stable state. The results shown below illustrate that the

eigenvalue-free small-signal stability criterion proposed in this paper is somewhat conservativeness compared with the GNC.

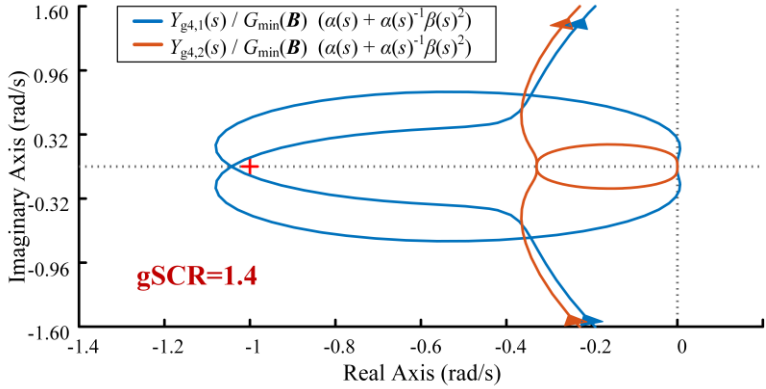

Figure 8: Generalized Nyquist curves of double-converter system under weak grid strength.

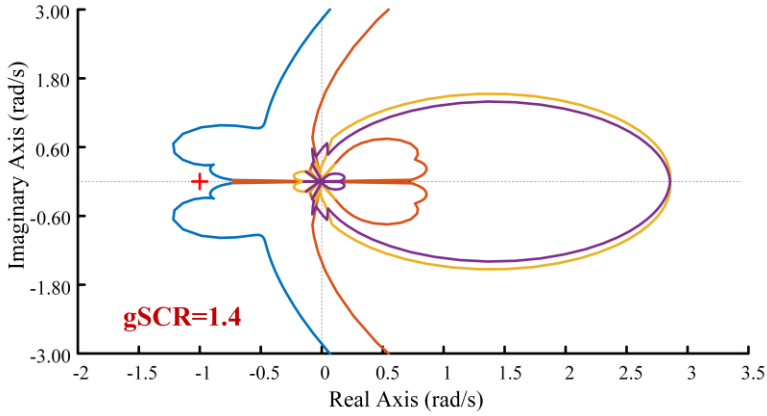

Figure 9: Generalized Nyquist curves for the double-converter system under weak grid strength.

4.3. The Influence of Different Weight Ratios on the Conservativeness of the Eigenvalue-Free Small-Signal Stability Criterion

Considering that the criterion proposed in this paper has a certain degree of conservativeness, in this section, a heuristic

exploration of the future development direction of this criterion is conducted through traversal to explore whether the device weighting method can reduce the conservation of the criterion proposed in this paper.

The following device weighting process is performed on the double-converter system in the modelling part.

$$\boldsymbol{Y}_{w,\delta} = m\boldsymbol{Y}_{g4,1} + n\boldsymbol{Y}_{g4,2}, m+n=1, \delta=1,2,\mathrm{L} \tag{30}$$

where, m and n are the weighting coefficients of VSC_1 and VSC_2 respectively, $\boldsymbol{Y}_{w,\delta}$ is the weighted converter.

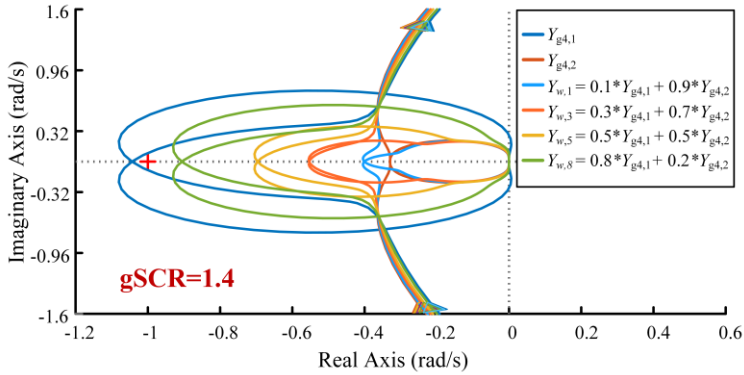

Figure 10: Proposed criterion of weighted converter system under weak grid strength.

Figure. 10 shows the influence of different weight ratios on the conservativeness of eigenvalue-free small-signal stability criterion under weak grid strength (gSCR=1.4). The above results show that the Nyquist curves of the criterion proposed in this paper under different weight ratios are within the range of the two curves of VSC_1 and VSC_2, and the conservativeness of the criterion can be reduced with the change of the weighting coefficient. This is because the eigenvalue-free small-signal stability criterion is a sufficient condition, which is a criterion obtained by drawing the Nyquist curves corresponding to the admittances of each converter one by one based on the minimum eigenvalue of the node admittance matrix $\boldsymbol{B}$.

4.4. Comparison and Analysis of Eigenvalue Calculation Results and Eigenvalue-Free Small-Signal Stability Criterion

Although Section 4.1 has demonstrated the effectiveness of Conclusion 2 through comparative analysis with the GNC, there is still a lack of more precise explanations for the adequacy of the eigenvalue-free small-signal stability criterion. In the following, the dominant eigenvalues of the system are supplemented according to the node admittance matrix in (29), and then the equation about the Laplacian operator s in (19) is calculated to obtain the distribution of system eigenvalues, as shown in Fig. 11.

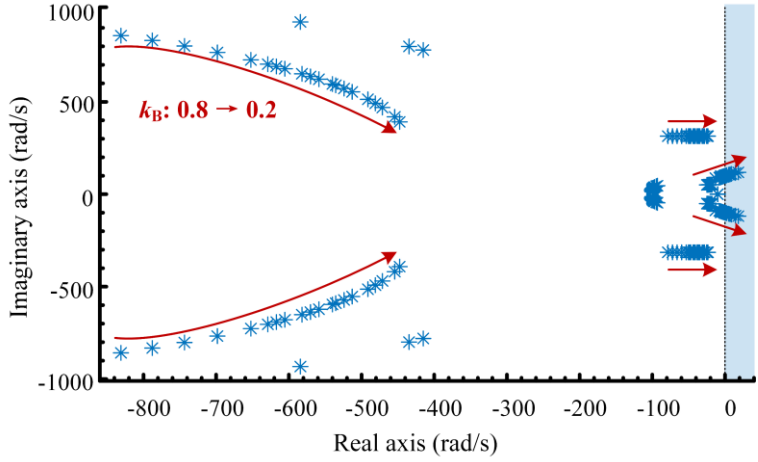

Figure11: Distribution of eigenvalues of double-converter system.

Specifically, by changing the node admittance matrix $\boldsymbol{B}$ and decreasing the parameter k_B from 0.8 to 0.2 in 0.01 per step, the power grid strength can be continuously declined. It can be seen that as the power grid strength decreases, the determinant zero point of the frequency-domain admittance matrix of the double-converter system gradually moves to the right half plane, and the stability of the system with small disturbance becomes worse.

It can be seen from Fig. 12 that the dominant eigenvalue of the system moves to the right half plane, varying from -10.84±89.8i to 13.89±68.52i, and the system changes from stable to unstable. Among them, when k_B is about 0.32, the dominant eigenvalue (0.12±86.2i) of the system is closest to the imaginary axis, which corresponds to the critical stability condition of the system.

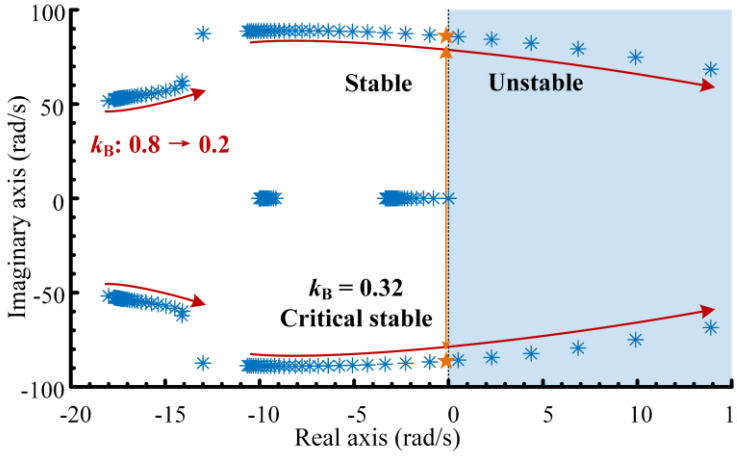

Figure 12: Variation trajectory of dominant eigenvalues of double-converter system.

Figure. 8 and Fig. 9 respectively depict the curves of the eigenvalue-free small-signal stability criterion and the GNC under weak grid strength. The eigenvalue-free small-signal stability criterion judges that the system is unstable, while the GNC judges that the system is stable. It is proved that the eigenvalue-free small-signal stability criterion in Conclusion 2 is a sufficient condition.

4.5. Double-converter System Time-Domain Simulation Verification

According to the double-converter topology shown in Fig. 5, the average model and detailed switching model are established respectively. The time-domain simulation analysis of the average value model is as follows, and the simulation results of the detailed switch model are shown in Appendix C.

If k_B=0.32, the system is critically unstable, and the output active and reactive power of the double-converter system is shown in Fig. 13. The results show that a subsynchronous oscillation of about 14.5 Hz occurs, which, together with the results in Fig. 8 and Fig. 9, shows that the eigenvalue-free small-signal stability criterion proposed in this paper can accurately identify the risk of system instability.

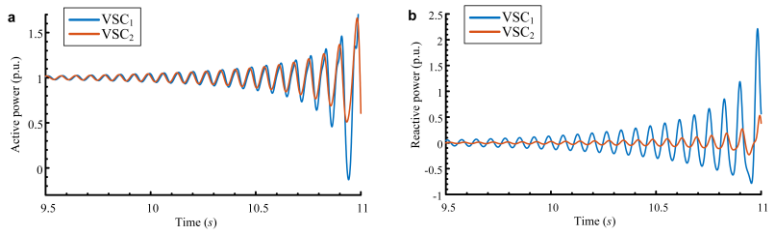

Figure 13: Time-domain simulation results of the double-converter system.

4.6. IEEE 39-Bus Test System Time-Domain Simulation Verification

To further verify the effectiveness of the proposed criterion, the topology of the IEEE 39-bus test system shown in Fig. 14 is adopted, and the synchronous generators in the original system are replaced with converters. Specifically, only the infinite bus with equivalent value through the external grid in the original system is retained, and the remaining synchronous generators are replaced with VSCs with a capacity of 1.0 p.u. The control parameters are shown in Table 3.

Table 3: Parameters of the IEEE 39-bus test system.

Symbols	Descriptions	Values
$PI_1(s)$	PLL transfer function of VSC_1, VSC_2 and VSC_9	26+7800/s
$PI_2(s)$	PLL transfer function of VSC_3 and VSC_4	36+7800/s
$PI_3(s)$	PLL transfer function of VSC_5 and VSC_6	26+3800/s
$PI_4(s)$	PLL transfer function of VSC_7 and VSC_8	36+3800/s

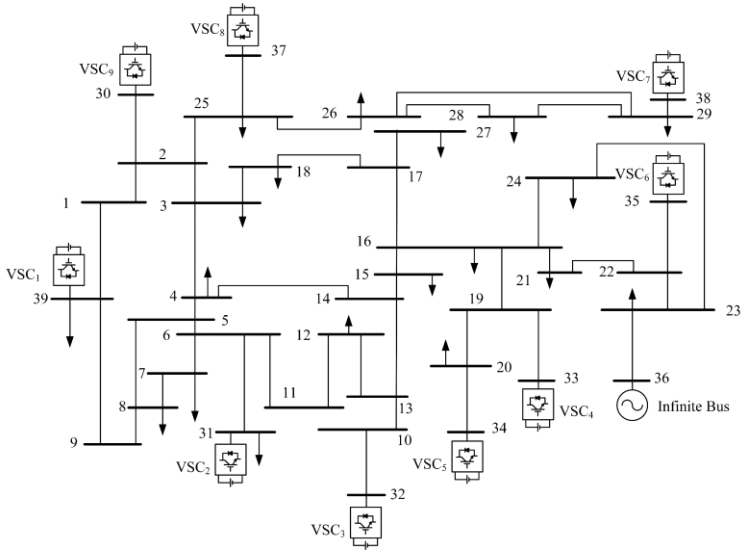

Figure 14: The IEEE 39-bus system.

Proportionally increasing the line parameters yields that the strength or gSCR of the IEEE 39-bus system is reduced to 1.43, resulting in the system time domain simulation curve shown in Fig. 14. It can be seen that the damping is very small, and the system is in a critical stable state.

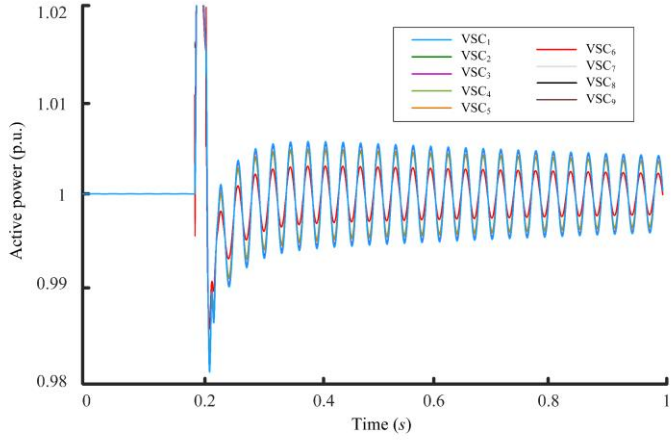

Figure15: Time-domain simulation results of the IEEE 39-bus system test system.

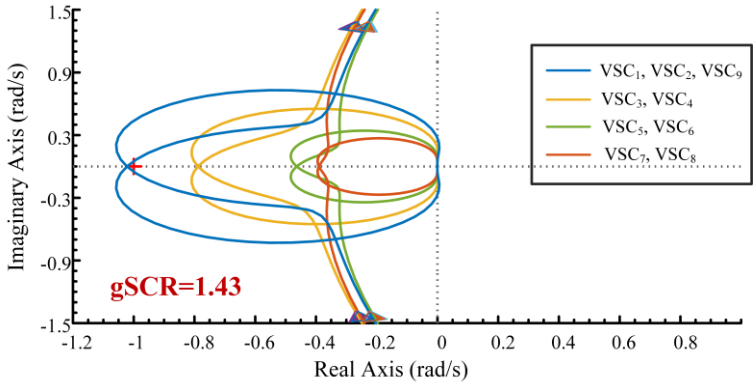

Figure16: Eigenvalue-free small-signal stability criterion of the IEEE 39-bus system test system (gSCR=1.43).

It can be seen from the results in Fig. 16 that when the gSCR of the system is 1.43, the criterion proposed in this paper is unstable. The time-domain simulation result in Fig. 15 shows that the system is close to critical stability under this gSCR, thus proving the criterion proposed in this paper is a sufficient condition for small-signal synchronization stability with applications to PLL-dominated oscillation mode analysis.

Furthermore, the proposed method is only related to device dynamics and system node admittance matrices $\boldsymbol{B}$, eliminating the need for calculating eigenvalues of the admittance matrix $\boldsymbol{Y}_{sys}$ at each frequency point, a requirement in methods like the GNC. This key distinction significantly reduces the computational burden associated with solving high-dimensional matrices during large network analysis.

Additionally, Fig. 16 illustrates that converters operating under identical control parameters exhibit identical curves. This observation suggests that, when the minimum eigenvalue of the node admittance matrix $\boldsymbol{B}$ is consistent, converters with the same control parameters located at different locations within the system exhibit equivalent stability. However, it's noteworthy that the method proposed in this paper has a limitation—it does not account for the influence of device location on overall system stability.

In summary, while the proposed method simplifies calculations by focusing on device dynamics and system node admittance matrices, it may not capture stability changes due to differences in device positions within the system.

5. Conclusion

Due to the large number and variety of converter controls, the GNC based on the eigenvalue trajectory is difficult to apply to the stability analysis of high-dimensional systems. To handle the problems of the heavy computational burden, poor observability and unclear physical meaning of the GNC for frequency domain admittance matrix of heterogeneous multi-converter systems, an eigenvalue-free small-signal stability criterion has been proposed. The analytical equation of the device weighting in the proposed criterion has revealed the stability mechanism of the multi-converter system as a compromise of the stability of each single-converter system. Moreover, the system frequency domain admittance matrix has been reduced to a SISO transfer function by using the numerical range and Gershgorin discs, which has resolved the problem of the large computational burden of high dimensional matrix eigenvalue solving. Finally, the criterion proposed in this paper is a sufficient condition for small-signal stability, but it is less conservative. In the future, the conservative property of the stability criterion can be reduced by reasonably setting the device weighting weight ratio under weak grids.

References

1. B Kroposki, Brian Johnson, Yingchen Zhang, Vahan Gevorgian, Paul Denholm. Achieving a 100% renewable grid: Operating electric power systems with extremely high levels of variable renewable energy. IEEE Power energy magazine. 2017; 15, 61-73.
2. S. Zhao, B Shao. An analytical method suitable for revealing the instability mechanism of power electronics dominated power systems. International Journal of Electrical Power & Energy Systems. 2019; 109: 269-282.
3. YJ Gu, TC Green. Power System Stability with a High

Penetration of Inverter-Based Resources. Proceedings of the IEEE. 2022.
4. S Golestan, JM Guerrero. Conventional synchronous reference frame phase-locked loop is an adaptive complex filter. IEEE Transactions on Industrial Electronics. 2014; 62: 1679-1682.
5. JZ Zhou, H Ding, S Fan, Y Zhang, AM Gole. Impact of Short-Circuit Ratio and Phase-Locked-Loop Parameters on the Small-Signal Behavior of a VSC-HVDC Converter. IEEE Transactions on Power Delivery. 2014; 29: 2287-2296.
6. X Wang, F Blaabjerg, W Wu. Modeling and Analysis of Harmonic Stability in an AC Power-Electronics-Based Power System," IEEE Transactions on Power Electronics. 2014; 29: 6421-6432,
7. D Wang, L Liang, L Shi, J Hu, Y Hou. Analysis of Modal Resonance Between PLL and DC-Link Voltage Control in Weak-Grid Tied VSCs. IEEE Transactions on Power Systems. 2019; 34:1127-1138.
8. LL Fan, ZX Miao. Wind in Weak Grids: 4 Hz or 30 Hz Oscillations?. IEEE Transactions on Power Systems. 2018; 33: 5803-5804.
9. D Dong, B Wen, D Boroyevich, P Mattavelli, YS Xue. Analysis of Phase-Locked Loop Low-Frequency Stability in Three-Phase Grid-Connected Power Converters Considering Admittance Interactions. IEEE Transactions on Industrial Electronics. 2015; 62: 310-321.
10. Z Wang, L Bao, L Fan, Z Miao, SJIToPS Shah, From Event Data to Wind Power Plant DQ Admittance and Stability Risk Assessment. IEEE Transactions on Power Systems. 2022.
11. M Amin, M Molinas. Small-Signal Stability Assessment of Power Electronics Based Power Systems: A Discussion of Admittance- and Eigenvalue-Based Methods. (in English), IEEE Transactions on Industry Applications. 2017; 53: 5014-5030.
12. J Liu, Wei Yao, Jinyu Wen, Jiakun Fang, Lin Jiang. Impact of Power Grid Strength and PLL Parameters on Stability of Grid-Connected DFIG Wind Farm. IEEE Transactions on Sustainable Energy. 2020; 11: 545-557.
13. W Du, W Dong, HFJIToPS Wang. Small-signal stability limit of a grid-connected PMSG wind farm dominated by the dynamics of PLLs. 2019; 35: 2093-2107.

14. B Wen, D Boroyevich, R Burgos, P Mattavelli, Z Shen. Analysis of DQ small-signal admittance of grid-tied inverters. IEEE Transactions on Power Electronics. 2016; 31: 675-687.
15. J Sun. Admittance-Based Stability Criterion for Grid-Connected Inverters. IEEE Transactions on Power Electronics. 2011; 26: 3075-3078.
16. Y Li, Zhikang Shuai, Xuan Liu, Yandong Chen, Zuyi Li. Stability Analysis and Location Optimization Method for Multiconverter Power Systems Based on Nodal Admittance Matrix. IEEE Journal of Emerging and Selected Topics in Power Electronics. 2021; 9: 529-538.
17. L Harnefors, M Bongiorno, S Lundberg. Input-Admittance Calculation and Shaping for Controlled Voltage-Source Converters. IEEE Transactions on Industrial Electronics. 2007; 54: 3323-3334.
18. S Shah, LJIToEC Parsa. Admittance modeling of three-phase voltage source converters in DQ, sequence, and phasor domains. 2017; 32: 1139-1150.
19. H Zhang, L Harnefors, X Wang, H Gong, J Hasler. Stability Analysis of Grid-Connected Voltage-Source Converters Using SISO Modeling. IEEE Transactions on Power Electronics. 2018; 1-1.
20. AGJ Macfarlane, I Postlethwaite. The generalized Nyquist stability criterion and multivariable root loci. International Journal of Control. 1977; 25: 81-127.
21. S Jiang, Y Zhu, GJIToPE Konstantinou. Settling-angle-based stability analysis for multiple current-controlled converters. 2022; 37: 12992-12997.
22. W Dong, H Xin, D Wu, L Huang. Small Signal Stability Analysis of Multi-Infeed Power Electronic Systems Based on Grid Strength Assessment," IEEE Transactions on Power Systems. 2019; 34: 1393-1403.
23. Y Zhou, Huanhai Xin, Di Wu, Feng Liu, Zhiyi Li. Small-Signal Stability Assessment of Heterogeneous Grid-Following Converter Power Systems Based on Grid Strength Analysis. in IEEE Transactions on Power Systems. 2023; 38: 2566-2579.
24. Jonsson E. Numerical Range of Square Matrices: A Study in Spectral Theory [J]. 2019.

25. So W, Thompson R C, Zhang F. The numerical range of normal matrices with quaternion entries [J]. Linear and Multilinear Algebra. 1994; 37: 175-195.

Appendix A

There are two frames in the converter grid-connected system: the *dq* control frame based on the PLL and the global *xy* frame. Among them, the *dq* frame rotates at the angular frequency ω measured by the PLL, and the *xy* frame rotates at the synchronous speed ω_0. The relationship between the two is shown in Fig. A. Similar to the derivation of the small-signal model of multi-synchronous machines in power systems, the dynamics of the converter in the *dq* control frame are first deduced, then transformed into global *xy* frame, and finally its admittance model is established in polar coordinates.

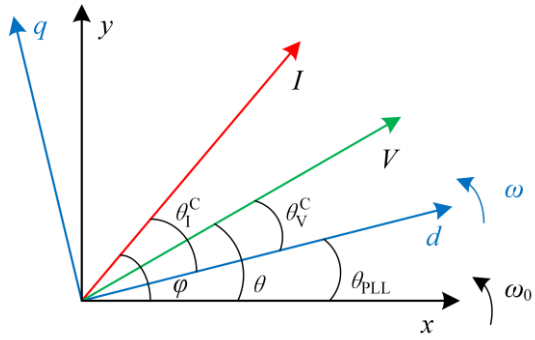

Figure A: Relationship between *dq* frame and *xy* frame.

By linearizing (3)-(5), the dynamic small-signal model of the filter inductor, PLL and converter inner loop in the *dq* frame can be obtained as:

Filter inductor dynamics:

$$\begin{cases} \Delta\dot{V}_{sd}^{*} - \Delta V_d = sL_f\Delta I_d - \omega_0 L_f \Delta I_q - L_f I_{q0}\Delta\omega \\ \Delta\dot{V}_{sq}^{*} - \Delta V_q = sL_f\Delta I_q + \omega_0 L_f \Delta I_d + L_f I_{d0}\Delta\omega \end{cases}$$

PLL dynamics:

$$\begin{cases} s\Delta\theta_{PLL} = PI_{PLL}(s)\Delta V_q \\ \Delta\omega = s\Delta\theta_{PLL} \end{cases}$$

Current inner loop dynamics:

$$\begin{cases} \Delta V_{sd}^{*} = (\Delta I_d^{ref} - \Delta I_d)PI_{CC}(s) - \omega_0 L_f \Delta I_q + f_{VF}(s)\Delta V_d \\ \Delta V_{sq}^{*} = (\Delta I_q^{ref} - \Delta I_q)PI_{CC}(s) - \omega_0 L_f \Delta I_d + f_{VF}(s)\Delta V_q \end{cases}$$

where, $PI_{PLL}(s)$ is the PLL transfer function of VSC, $PI_{CC}(s)=K_{CCP}+K_{CCI}/s$ is the current inner loop PI controller transfer function, $f_{VF}(s)=K_{VF}/(T_{VF}s+1)$ is a voltage feedforward low-pass filter.

Substituting (A2) into (A1) and (A3), the relationship between current and voltage in *dq* frame can be obtained by:

$$\begin{cases} \Delta I_d = -\dfrac{1-f_{VF}(s)}{sL_f + PI_{CC}(s)}\Delta V_d + \dfrac{L_f PI_{PLL}(s) I_{q0}}{sL_f + PI_{CC}(s)}\Delta V_q + \dfrac{PI_{CC}(s)}{sL_f + PI_{CC}(s)}\Delta I_d^{ref} \\ \Delta I_q = -\dfrac{1-f_{VF}(s)}{sL_f + PI_{CC}(s)}\Delta V_q - \dfrac{L_f PI_{PLL}(s) I_{d0}}{sL_f + PI_{CC}(s)}\Delta V_q + \dfrac{PI_{CC}(s)}{sL_f + PI_{CC}(s)}\Delta I_q^{ref} \end{cases}$$

By linearizing the outer loop dynamic equations (6)-(11), the dynamic small signal model of converter outer loop in the dq frame can be obtained as:

Reactive power outer loop:

$$\Delta I_q^{\text{ref}} = PI_{QC}(s)\, f_{PQ}(s)\Delta Q_e$$

Constant active power control:

$$\Delta I_d^{\text{ref}} = -PI_{PC}(s)\, f_{PQ}(s)\Delta P_e$$

Constant DC voltage control:

$$sV_{\mathrm{dc0}}C_{\mathrm{dc}}\Delta V_{\mathrm{dc}} = -\Delta P_{\mathrm{e}}$$

Power equation:

$$\begin{bmatrix}\Delta P_e\\ \Delta Q_e\end{bmatrix} = \begin{bmatrix}V_{d0} & \\ & -V_{d0}\end{bmatrix}\begin{bmatrix}\Delta I_d\\ \Delta I_q\end{bmatrix} + \begin{bmatrix}I_{d0} & I_{q0}\\ -I_{q0} & I_{d0}\end{bmatrix}\begin{bmatrix}\Delta V_d\\ \Delta V_q\end{bmatrix}$$

Substituting (A5)-(A8) into (A4), the admittance characteristics of the converter port in *dq* frame is shown below (Suppose the current flowing into the converter is in the positive direction)：

$$\begin{bmatrix}\Delta I_d\\ \Delta I_q\end{bmatrix} = \begin{bmatrix}\dfrac{G_{\mathrm{VF}}(s)+G_{\mathrm{I}}(s)G_{\mathrm{APC}}(s)I_{\mathrm{d0}}}{G_{\mathrm{I}}(s)G_{\mathrm{APC}}(s)V_{\mathrm{d0}}+1} & \dfrac{-\frac{PI_{PLL}(s)}{s}(1-G_I(s))I_{\mathrm{q0}}+G_{\mathrm{APC}}(s)G_{\mathrm{I}}(s)I_{\mathrm{q0}}}{G_{\mathrm{I}}(s)G_{\mathrm{RPC}}(s)V_{\mathrm{d0}}+1}\\ \dfrac{G_{\mathrm{I}}(s)G_{\mathrm{RPC}}(s)I_{\mathrm{q0}}}{G_{\mathrm{I}}(s)G_{\mathrm{APC}}(s)V_{\mathrm{d0}}+1} & \dfrac{G_{\mathrm{VF}}(s)+\frac{PI_{PLL}(s)}{s}(1-G_I(s))I_{\mathrm{d0}}-G_{\mathrm{RPC}}(s)G_{\mathrm{I}}(s)I_{\mathrm{d0}}}{G_{\mathrm{I}}(s)G_{\mathrm{RPC}}(s)V_{\mathrm{d0}}+1}\end{bmatrix}\begin{bmatrix}\Delta V_d\\ \Delta V_q\end{bmatrix} \quad \text{(A9)}$$
$$= \begin{bmatrix}Y_{dd}(s) & Y_{dq}(s)\\ Y_{qd}(s) & Y_{qq}(s)\end{bmatrix}\begin{bmatrix}\Delta V_d\\ \Delta V_q\end{bmatrix}$$

where, the subscript '0' of the physical quantity indicates the steady-state value of the physical quantity: $V_{\mathrm{d0}}=1.0\mathrm{p.u.}$, $I_{\mathrm{d0}}=1.0\mathrm{p.u.}$, etc.; the transfer function G_{xx} is given as below:

$$\begin{cases}G_{\mathrm{RPC}}(s)=PI_{\mathrm{QC}}(s)\,f_{\mathrm{PQ}}(s)\\ G_{\mathrm{VF}}(s)=(1-f_{\mathrm{VF}}(s))/(sL_{\mathrm{f}}+PI_{\mathrm{CC}}(s))\\ G_{\mathrm{I}}(s)=PI_{\mathrm{CC}}(s)/(sL_{\mathrm{f}}+PI_{\mathrm{CC}}(s))\\ G_{\mathrm{APC}}(s)=\begin{cases}PI_{\mathrm{DC}}(s)/sV_{\mathrm{dc0}}C_{\mathrm{dc}}, \text{ Constant DC voltage outer loop}\\ PI_{\mathrm{PC}}(s)\,f_{\mathrm{PQ}}(s), \text{ Constant active power outer loop}\end{cases}\end{cases}$$

According to Fig. A, the conversion relationship between voltage and current between the *dq* frame and the *xy* frame can be obtained:

$$\begin{bmatrix}V_d\\ V_q\end{bmatrix} = \begin{bmatrix}\cos\theta_{PLL} & -\sin\theta_{PLL}\\ \sin\theta_{PLL} & \cos\theta_{PLL}\end{bmatrix}\begin{bmatrix}V_x\\ V_y\end{bmatrix}$$
$$\begin{bmatrix}I_d\\ I_q\end{bmatrix} = \begin{bmatrix}\cos\theta_{PLL} & -\sin\theta_{PLL}\\ \sin\theta_{PLL} & \cos\theta_{PLL}\end{bmatrix}\begin{bmatrix}I_x\\ I_y\end{bmatrix}$$

Linearize (A10) and combine with (A2), the conversion relationship between voltage and current between the *dq* frame and the *xy* frame can be rewritten as:

$$\begin{bmatrix}\Delta V_d\\ \Delta V_q\end{bmatrix}=\begin{bmatrix}1 & \\ & 1-G_{PLL}(s)\end{bmatrix}\begin{bmatrix}\Delta V_x\\ \Delta V_y\end{bmatrix}$$
$$\begin{bmatrix}\Delta I_d\\ \Delta I_q\end{bmatrix}=\begin{bmatrix}\Delta I_x\\ \Delta I_y\end{bmatrix}+\begin{bmatrix}0 & G_{PLL}(s)I_{q0}\\ 0 & -G_{PLL}(s)I_{d0}\end{bmatrix}\begin{bmatrix}\Delta V_x\\ \Delta V_y\end{bmatrix}$$

where, $G_{\mathrm{PLL}}(s)=\dfrac{PI_{\mathrm{PLL}}(s)}{s}/(1+\dfrac{PI_{\mathrm{PLL}}(s)V_{\mathrm{d0}}}{s})$.

Then, substitute (A11) into (A9) to obtain the admittance matrix of the converter in global *xy* frame:

$$\begin{bmatrix}\Delta I_x\\ \Delta I_y\end{bmatrix}=\underbrace{\begin{bmatrix}\dfrac{G_{\mathrm{VF}}(s)+G_{\mathrm{I}}(s)G_{\mathrm{APC}}(s)I_{\mathrm{d0}}}{G_{\mathrm{I}}(s)G_{\mathrm{APC}}(s)+1} & \dfrac{(G_{\mathrm{PLL}}(s)+G_{\mathrm{APC}}(s))G_{\mathrm{I}}(s)I_{\mathrm{q0}}}{G_{\mathrm{I}}(s)G_{\mathrm{RPC}}(s)+1}\\ \dfrac{G_{\mathrm{I}}(s)G_{\mathrm{RPC}}(s)I_{\mathrm{q0}}}{G_{\mathrm{I}}(s)G_{\mathrm{RPC}}(s)+1} & \dfrac{(1-G_{\mathrm{PLL}}(s))G_{\mathrm{VF}}(s)-(G_{\mathrm{PLL}}(s)+G_{\mathrm{RPC}}(s))G_{\mathrm{I}}(s)I_{\mathrm{d0}}}{G_{\mathrm{I}}(s)G_{\mathrm{RPC}}(s)+1}\end{bmatrix}}_{\boldsymbol{Y}_{\mathrm{VSC}}^{xy}(s)}\begin{bmatrix}\Delta V_x\\ \Delta V_y\end{bmatrix} \quad \text{(A12)}$$

According to Fig. A, it can be seen that the conversion relationship between the rectangular coordinates and the polar coordinates of voltage/current in the *xy* frame is:

$$\begin{cases}V_x=V\cos\theta, I_x=I\cos\varphi\\ V_y=V\sin\theta, I_y=I\sin\varphi\end{cases} \quad \text{(A13)}$$

Finally, linearize (A13) and combine with (A12), the dynamic equation of the converter in the polar coordinates can be obtained:

$$\begin{bmatrix}\Delta I\\ I\Delta\varphi\end{bmatrix}=T^{-1}(\varphi)\boldsymbol{Y}_{VSC}^{xy}(s)T(\theta)\begin{bmatrix}\Delta V\\ V\Delta\theta\end{bmatrix} \quad \text{(A14)}$$

where, $T(\delta)=\begin{bmatrix}\cos\delta & -\sin\delta\\ \sin\delta & \cos\delta\end{bmatrix}$, $\delta=\varphi$ or $\delta=\theta$.

If the *xy* frame is chosen so that the steady-state voltage V coincides with the x-axis, then $\theta_{\mathrm{PLL}} = \theta = 0$. Therefore, under unit power factor, the admittance matrix $\boldsymbol{Y}_{\mathrm{VSC}}(s)$ of the converter in polar coordinates is shown below:

$$\begin{bmatrix} \Delta I \\ I\Delta\varphi \end{bmatrix} = \underbrace{\begin{bmatrix} Y_{g1} & \\ & Y_{g4} \end{bmatrix}}_{\boldsymbol{Y}_{\mathrm{VSC}}(s)} \begin{bmatrix} \Delta V \\ V\Delta\theta \end{bmatrix} \tag{A15}$$

where, $\begin{cases} Y_{g1}(s) = \dfrac{G_{\mathrm{VF}}(s) + G_{\mathrm{I}}(s)G_{\mathrm{APC}}(s)I_{\mathrm{d0}}}{G_{\mathrm{I}}(s)G_{\mathrm{APC}}(s)V_{\mathrm{d0}} + 1} \\ Y_{g4}(s) = \dfrac{G_{\mathrm{VF}}(s)(1 - V_{\mathrm{d0}}G_{\mathrm{PLL}}(s))}{G_{\mathrm{I}}(s)G_{\mathrm{RPC}}(s)V_{\mathrm{d0}} + 1} - \dfrac{(G_{\mathrm{RPC}}(s) + G_{\mathrm{PLL}}(s))G_{\mathrm{I}}(s)I_{\mathrm{d0}}}{G_{\mathrm{I}}(s)G_{\mathrm{RPC}}(s)V_{\mathrm{d0}} + 1} \end{cases}$.

Appendix B

The return deference matrix of homogeneous multi-converter system in [22] is shown below.

$$\boldsymbol{Y}_{sys} = \boldsymbol{Y}_{grid}(s) + \boldsymbol{Y}_{g}(s) \tag{B1}$$

where

$$\boldsymbol{Y}_{grid}(s) = \boldsymbol{B} \otimes \begin{bmatrix} \alpha(s) & \beta(s) \\ -\beta(s) & \alpha(s) \end{bmatrix} \tag{B2}$$

$$\boldsymbol{Y}_{g} = \boldsymbol{I} \otimes \begin{bmatrix} Y_{g1}(s) & \\ & Y_{g4}(s) \end{bmatrix} \tag{B3}$$

When rearrange the matrix elements, the return deference matrix of heterogeneous multi-converter system is obtained as follows.

$$\det(\boldsymbol{Y}_{sys}) = \det\left(\begin{bmatrix} \boldsymbol{Y}_{g1} & \\ & \boldsymbol{Y}_{g4} \end{bmatrix} + \begin{bmatrix} \boldsymbol{B}\alpha(s) & \boldsymbol{B}\beta(s) \\ -\boldsymbol{B}\beta(s) & \boldsymbol{B}\alpha(s) \end{bmatrix} \right) \tag{B4}$$

According to Fig. 2, except for the phase loop element $Y_{g(2,2)}(s)$ represented in the lower right corner, the amplitudes of the other three elements in the sub/supersynchronous oscillation frequency band (10Hz~100Hz) are less than 0 dB, so these three elements

can be ignored (i.e. Y_{g1} can be ignored). Hence, the system frequency domain admittance matrix Y_{sys} of the multi-converter system can be obtained by:

$$\begin{bmatrix} \boldsymbol{Y}_{g1}+\boldsymbol{B}\alpha(s) & \boldsymbol{B}\beta(s) \\ -\boldsymbol{B}\beta(s) & \boldsymbol{Y}_{g4}+\boldsymbol{B}\alpha(s) \end{bmatrix} \approx \begin{bmatrix} \boldsymbol{B}\alpha(s) & \boldsymbol{B}\beta(s) \\ -\boldsymbol{B}\beta(s) & \boldsymbol{Y}_{g4}+\boldsymbol{B}\alpha(s) \end{bmatrix} = \boldsymbol{Y}_{sys} \tag{B5}$$

Appendix C

A detailed switch model of a double-converter system containing switches and three-phase circuits is built through Matlab/Simulink. The parameters of the double-converter system are shown in Table 2. The three-phase terminal voltages of VSC_1 and VSC_2 are demonstrated in Fig. B and Fig. C, respectively.

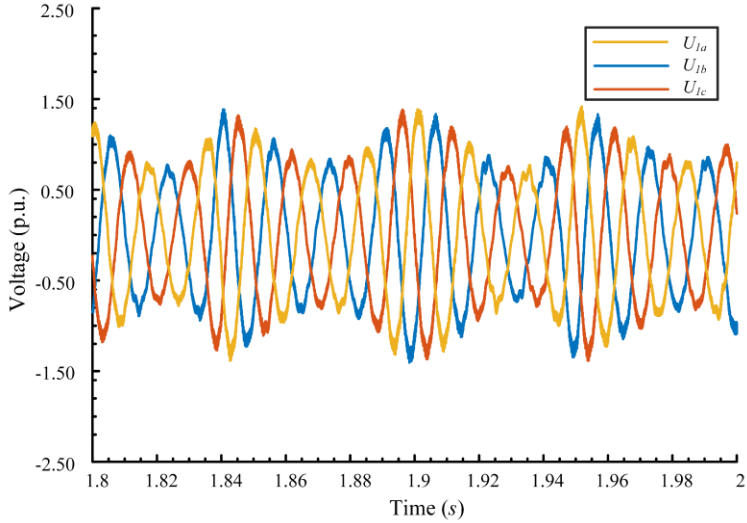

Figure B: Three-phase terminal voltage of VSC_1.

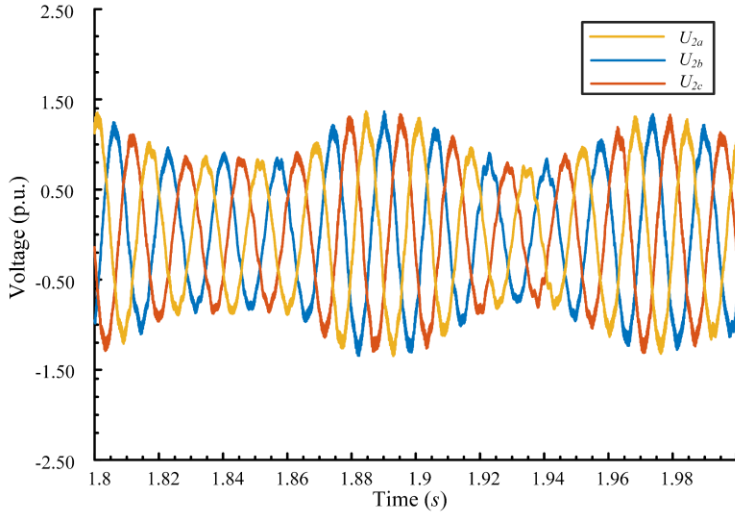

Figure C: Three-phase terminal voltage of VSC_2.